②

University of Notre Dame

Aerospace and Mechanical Engineering
365 Fitzpatrick Hall of Engineering

Notre Dame, Indiana 46556-9956
Telephone: (219) 239-5430
Fax: (219) 239-8007

AD-A220 298

Dr. S.G. Lekoudis
Scientific Officer, Fluid Dynamics
Department of the Navy
Office of Naval Research
Code 1132-F
800 North Quincy Street
Arlington, Virginia 22217

Subject: Annual Report for the period 1 April 1989 to 31 March 1990, Contract Number N00014-89-J-1783, Fluid Dynamic and Acoustic Experiments on Turbomachine Rotors Subject to Variable Flow Conditions

Dear Sir:

The primary objective of this research is to obtain a better understanding of how inflow nonuniformities interact with rotor blades, thereby producing rotor vibrations and the radiation of unwanted noise. In this research, carefully controlled experiments will be conducted in low speed wind tunnels utilizing an advanced rotor-dynamometer system. The fluid mechanical characteristics of the inflow will be documented and related to performance and blade radiated sound. The blade response, as characterized by its thrust, torque, surface pressure distribution and radiated sound, will be measured for the cases of both steady and unsteady inflows of variable turbulence intensity and scale.

I. ROTOR-DYNAMOMETER PERFORMANCE MEASUREMENTS

a. Description of Research

A foremost consideration in experiments designed to determine how various inflow nonuniformities interact with rotor blades is the response of the rotor itself to both steady and nonsteady disturbances. A complete characterization of rotor response requires the measurement of the rotor's thrust, torque and rpm, and individual blade loading as a function of inflow conditions. Typically, this is accomplished best by determining the rotor's thrust and torque coefficients and blade surface pressure distribution as a function of rotor advance ratio. The accurate measurement of each of these parameters can be achieved through use of the advanced rotor-dynamometer developed for this project.

Our approach in incorporating the advanced rotor-dynamometer into this research program chronologically consists of four stages: (1) design, fabricate, shakedown the dynamometer, (2) use the dynamometer in a series of rotor-dynamometer performance studies, in which the rotor response is characterized in terms of its efficiency, torque and thrust coefficients versus advance ratio under steady inflow conditions, and the structure of the flow about the rotor is characterized using various flow visualization techniques, (3) perform similar experiments to those in the second

stage in which the rotor is operated in a duct, and (4) conduct experiments similar to those in the second and third stages in which the effect of upstream turbulence intensity (between 0.07% and 5.0%) on performance will be determined, and acoustic measurements will be made to ascertain the influence of the turbulence length scale at the same intensity and its relation to the radiated noise spectrum. This contract year, we completed the first two stages. The results of this effort are described in the following.

b. Significant Results since 1 April 1989

During the first six months of this project, we designed and fabricated the advanced rotor-dynamometer and then conducted initial shakedown tests in a low speed wind tunnel. This completed the first stage of our plan. During the second six months, we used this dynamometer to characterize the forward and backing operating performances of an unducted #3714 four-bladed propeller that was tested previously at the NSRDC.This completed the second stage of our plan.

i. The Advanced Rotor-Dynamometer

The advanced rotor-dynamometer was designed to utilize state-of-the-art components to achieve the accurate measurement of rotor rpm, torque and displacement. This dynamometer, capable of either forward or aft-mounted rotor configurations, was carefully constructed with high precision bearings, couplings and instrumentation to provide very accurate performance measurements.Using this device, rotor rpm, torque and displacement can be measured to within 0.001%, 1.5% and 3.2% accuracy, respectively, over a typical advance ratio range. When used in a low speed wind tunnel, the resultant average errors in the thrust coefficient, torque coefficient, efficiency and advance ratio are 3.5%, 2.1%, 4.2% and 1.2%, respectively. This type of accuracy is achieved through use of an optical encoder to determine rpm, an optical torque meter, and a Linearly Variable Differential Transformer (LVDT) to measure displacement. Each instrument is linked to its own signal conditioning unit, which, in turn, is connected through an A/D board to a MacIntosh II computer. In this manner, the rotor's performance parameters can be determined and viewed in real-time and recorded over a wide range of inflow conditions.

The advanced dynamometer system, shown schematically in Figure 1, is comprised of the dynamometer itself, which is mounted in a wind tunnel test section, the required external signal conditioning and operational control units, a Macintosh II computer utilized for its data acquisition abilities, and, of course, the actual wind tunnel facility.

The propeller dynamometer itself is comprised of a servomotor, optical torque transducer, LVDT thrust sensor, dynamometer shaft assembly and two aluminum shaft couplings. These components are all housed within an aluminum casing which is mounted in a wind tunnel for operation. A brushless servomotor is mounted in the rear of the dynamometer. This motor is equipped with a resolver which allows for very accurate position and speed control. The resolver eliminates the need for contact brushes which result in internal system friction and motor wear.

The motor is a compact 2.0 in. diameter, 8.38 in. long Pacific Scientific brushless model R23HENA-R1-NS-NV-00 samarium-cobalt permanent magnet servomotor. An operating range of 0 to ±8,000 rpm is possible with a speed resolution of ±0.01 rpm. The motor can deliver 14 lb-in. peak stall torque and 7.6 lb-in. continuous stall torque. With a 230 VAC input voltage, the servomotor controller is capable of up to 1000 W continuous stall power and 2000 W peak power. Its current output is rated at 3.5 A continuous stall current and 7.0 A peak current. Position control resolution is rated at 4096 steps per revolution with an accuracy of ±0.001 revolutions.

The motor shaft is connected to an optical torque transducer with a solid aluminum shaft coupling. The aluminum shaft coupling exhibits very little backlash ensuring that nearly all the torque output by the motor is transmitted through the rest of the system. The optical torque transducer is a very sensitive and accurate device for measuring torque. It is equipped with two optical disks that are mounted on a torsion bar within the unit. Rotation of the slotted disks relative to each other alters the "window area" between lamps and photoelectric cells, developing an output current proportional to torque. The disks are initially positioned on the torque bar to give a 50%

overlap between transparent and opaque segments. This allows the system output to be torque directional and also allows the instrument to work on the most linear portion of its calibration output curve.

The optical torque transducer is a Vibrac series I TQ100DS. It has a full scale torque rating of 100 oz-in. with linearity, hysteresis, ripple and calibration accuracies of ±0.25% of full-scale each. The overall accuracy of the torque transducer is rated at ±1% of full-scale. The optical torque transducer was purchased with a readout and control unit.

Another aluminum shaft coupling is used to connect the optical torque transducer to the dynamometer shaft. As can be seen in the detailed drawing of the dynamometer system provided in Figure 2, the dynamometer shaft extends through the LVDT coil assembly and transmits torque to the propeller shaft via a transverse shaft. Expanded views of the dynamometer shaft and propeller shaft are shown in Figure 3 to help define how the two shafts interconnect. The propeller shaft slides LVDT core end first into the dynamometer shaft. The transverse shaft is then inserted along with Fafnir SSRI-614 radial bearings which define the range of motion for the LVDT thrust measurement sensor.

High precision New Hampshire Ball Bearings, Inc. RI-542KF deep groove torque bearings allow the propeller shaft to rotate as a unit with the dynamometer shaft while the Miniature Bearings, Inc. Rotolin ML500-875-1 precision linear bearings allow the propeller shaft to translate in the horizontal (axial) direction within the dynamometer shaft. The LVDT core has been fixed to the end of the propeller shaft such that the displacement produced by the propeller can be measured by the LVDT. The portion of dynamometer shaft that extends through the LVDT coil has been constructed out of a phenolic material to avoid external magnetic eddy current effects that would interfere with the output of the LVDT.

Very accurate thrust measurements are made possible due to the accuracy of the LVDT to measure linear displacement. An LVDT consists of one primary and two secondary coils symmetrically spaced on a cylindrical form. When the primary coil is excited by an external AC source, voltages are induced in the two secondary coils due to a free-moving rod-shaped magnetic core that provides a path for the magnetic flux linking the coils. The transducer's output is simply the difference between the induced voltages within the secondary coils, which varies linearly with the changes in-core position. The overall range of the LVDT voltage output is 10 V. Referring to Figure 2, a spring and adjustable mounting nut on the propeller shaft provide the necessary counter force to retain the propeller shaft assembly from extending out of the linear range of the LVDT.

The Linearly Variable Differential Transformer is a Schaevitz Engineering Model 503XS-A with a linear range of ±0.5 in. The XS-A series is characterized by a large mechanical separation between the LVDT coil and core. This is required to allow space for the passage of the dynamometer shaft assembly which transmits torque to the propeller shaft. Internal magnetic and electrostatic shielding render the XS-A insensitive to external magnetic influences. The LVDT requires an input voltage of 3 Vrms and operates in a frequency range of 400 Hz to 5 kHz. The LVDT has a linearity rating of ±0.5% of full range and a sensitivity of 0.6 mV out per volt excitation per 0.001 in. displacement. The impedance of the primary and secondary coils are 460 and 3200 ohms, respectively.

The entire dynamometer is supported by two cylindrical struts that mount directly to the wind tunnel test section floor. All of the electrical leads from the system components are fed along the rear of the dynamometer housing and out of the test section floor to the external conditioning and control units.

External of the wind tunnel test section, which holds the propeller dynamometer system while conducting propeller performance tests, are the various measurement instrumentation conditioning units and control units. These devices consist of a Setra Systems Model 339H electronic manometer for measuring wind tunnel flow velocity, a Pacific Scientific Model SC452-002-03 digital position and velocity motor control unit, the LVDT power supply and operating circuitry and a Vibrac TM72-18 digital torque measurement instrument.

The Setra Systems electronic manometer is used in conjunction with a standard pitot tube that is mounted in the wind tunnel test section upstream of the dynamometer system. The

manometer has a pressure measurement range of 0 to ±0.5536 in. H2O with an overall accuracy of ±1.4% full-scale. This manufacturer's listed accuracy results in a ±0.0078 in. H2O resolution. A 0 to 5V output range necessitates a 0.11072 in. H2O/V conversion factor for use in data acquisition.

The Pacific Scientific digital position and velocity control unit was purchased with the Pacific Scientific brushless servomotor. The control unit operates the motor through user input PacSci Motion BASIC computer codes. PacSci Motion BASIC is based on the BASIC programming language but utilizes fewer structural abilities and incorporates more generic command syntax. A "dummy" terminal is used to enter the necessary commands for motor operation. This terminal utilizes an RS232 communications port to "talk" with the control unit. Currently, the dynamometer system data acquisition software, executed on a Macintosh II computer, is not capable of accepting or transmitting signals along the Macintosh II's RS232 port.

Operation of the LVDT thrust sensor is achieved through an external circuit board. A power supply unit provides a frequency generator chip with the proper input voltage needed to generate a sine wave voltage output of approximately 5 kHz amplitude. This sine wave voltage is sent to the primary coil of the LVDT sensor. The sensor output signal, received from the secondary coils, is amplified and then sent through an RMS to DC converter. The final DC output is then available to be read by the data acquisition software. The external circuit board also incorporates a zeroing potentiometer and maximum voltage output potentiometer for calibration requirements.

A Vibrac TM72-18 torque measurement instrument contains the driving circuitry for the optical torque transducer's optics as well as provides a digital torque output. This unit was purchased with the Vibrac optical torque transducer. The TM72-18 has a manufacturer's listed accuracy of ±0.5% of full-scale output and torque transducer accuracy. A 10 VDC output port provides the necessary means for the data acquisition software to read the dynamometer system torque.

Analog voltage signals from the electronic manometer, LVDT thrust sensor and torque meter are read and manipulated by a National Instruments, Inc. NB-MIO-16H A/D board inside a Macintosh II computer. The inputs are manipulated and stored in the computer which utilized LabVIEW software. LabVIEW (Laboratory Virtual Instrument Engineering Workbench) has been designed by National Instruments Corporation to simplify programming scientific computation, process control, and test and measurement applications. LabVIEW allows the programmer to determine the number and rate of data samples taken during the data acquisition period. Currently, four channels are read by the A/D board sequentially with 750 A/D conversions per channel. An average of these 750 data points is determined and recorded as one performance data point. The analog voltage readings were converted directly into propeller performance coefficients using a LabVIEW program developed for this project. In this program, C_T, C_Q, η, and J are all calculated and displayed after entering the rpm for the condition tested, and the room temperature and atmospheric pressure at the beginning of the test, . The performance characteristics are also stored in a data file along with the raw voltage signals and voltage signal standard deviations.

ii. #3714 Performance Characterization Experiments

Dynamometer Measurements:

All of the #3714 propeller performance characterization experiments were conducted in a subsonic, indraft, low-turbulence wind tunnel located at the University of Notre Dame Aerospace Engineering Laboratory. The thesis research of Asson (1990) comprised a majority of this work. A schematic of the tunnel is shown in Figure 4. The inlet has 12 anti-turbulence screens and a 24:1 contraction ratio. The anti-turbulence screens result in a uniform velocity profile in the test section and a free-stream turbulence intensity of less than 0.1%. The wind tunnel is capable of flow velocities up to 100 ft/s. A more complete description of the wind tunnel facilities at the University of Notre Dame is provided by Mueller (1983).

First, the "ahead" propeller performance characteristics for this 10 in. diameter, four-bladed marine propeller having a pitch-to-diameter ratio of 1.262 were measured. Three tests were conducted in one experimental session during which one test immediately following the other, and

then another two tests were performed under the exact conditions on a different day. Before and after each experiment, a tare torque calibration and LVDT thrust sensor spring calibration were performed. Each experiment with the propeller was conducted at a propeller shaft rotation of 3000 rpm.With the previous Navy data as a guide, an advance ratio range of J=0.3 to J=1.3 was chosen for all of these measurements. An LVDT thrust sensor retention spring of stiffness k=1.50 in./lb was chosen for these tests because of its ability to allow full range extension of the propeller shaft for the range of advance ratios being studied.

The performance of a propeller can be directly related to its C_T, C_Q and η. These dimensionless quantities are defined as:

$$C_T = \frac{T}{\rho n^2 D^4} \qquad (1)$$

$$C_Q = \frac{Q}{\rho n^2 D^5} \qquad (2)$$

$$\eta = \frac{P_a}{P} = \frac{TV_\infty}{2\pi nQ} = \frac{C_T J}{2\pi C_Q} \qquad (3)$$

where P_a, in Equation 3, is the power available from the propeller and P is the power delivered to the propeller. In the above equations, ρ is the density of the fluid in which the propeller is operating, n is the rotational speed of the propeller and D is the propeller diameter.

Figure 7 shows the "ahead" performance characteristics, i.e., the thrust and torque coefficients, and the efficiency, of the propeller as a function of J. Results obtained from the NSRDC experiments in water are shown for comparison. Slightly higher C_T values and slightly lower C_Q values were measured by the new propeller dynamometer system in the wind tunnel, which in turn account for the slightly higher values of η when compared to the NSRDC data. The general trend of the C_T shows that at low J, where the speed of advance of the air flow is low, the propeller is generating relatively large amounts of thrust. This is due to the large transfer of momentum between the fast rotating propeller blades and slow moving air, a direct result of the relative high angle of attack of the propeller blades to the free-stream flow. At high J, where the speed of advance of the air flow is greater, the relative angle of attack of the free-stream flow seen by the propeller is decreased resulting in lower propeller thrust output.

The C_Q measured by the new propeller dynamometer system in air agrees very closely with the NSRDC data taken in the water. At low J, higher torque input is required by the dynamometer motor to maintain the 3000 rpm shaft rotation. This is due to the relatively low speed of advance of the air flow which limits the ability of the air to impart rotational energy to the propeller. As J increases, the speed of advance of the air flow increases, providing a greater transfer of energy from the air flow to the propeller. This increase in rotational energy provided by the air flow into the propeller reduces the input torque required of the dynamometer motor.

A maximum efficiency of approximately η=0.89 is attained at J=1.1 for "ahead " operation. As can be seen in Figure 7, η increases with increasing J until approximately J=1.1, and then sharply decreases with further increase in J. Using the definition of propeller efficiency (Equation 3), several comments can be made about the η trend shown in Figure 7. At low J, the advance of the free-stream flow, V_∞, is slow providing for a small contribution to the power available $(P_a=T_aV_\infty)$ of the propeller. Because $\eta = P_a/P$, where P is the power delivered to the propeller, η is low at low J. As J is increased, the free-stream flow velocity increases, correspondingly increasing the P_a of the propeller. Because the power required by the propeller operating at a constant rpm decreases as V_∞ increases, the efficiency has to increase. At high J, the propeller

loses lift due to the small angles of attack between the propeller blades and the relative free-stream flow. With this decrease in T_a from the propeller, the P_a decreases which accounts for the decrease in η.

Figure 8 shows the results of the third experiment conducted in a series during the same testing session. Again a slightly higher C_T was measured as compared to the NSRDC data. Figure 8 also shows a less consistent C_Q measurement in comparison with the results provided in Figure 7. This C_Q discrepancy is attributed to a measured tare torque of 0.021 N-m prior to this final test as compared to a measured tare torque of 0.015 N-m for the first two tests conducted. When subtracted from the torque measurements this higher tare torque value results in a C_Q slightly less than the C_Q results shown in Figure 7.

Upon completion of this third test, another tare torque calibration was performed which resulted in a measured tare torque of 0.015 N-m, which was the same tare torque measured prior to the first and second tests conducted. It was concluded that the high tare torque measurement recorded prior to the third test was most likely the result of an adjustment made to one of the dynamometer's couplings. Ample running time was not allowed to "re-set" the dynamometer bearings before continuing with the final test, resulting in the higher measured tare torque and lower overall C_Q. Figure 9 shows the same C_Q values obtained from the third test corrected with a tare torque value of 0.015 N-m. This C_Q shows better agreement between the measured data and the NSRDC results, which supports the aforementioned conclusion.

Several more propeller performance characteristic tests on the propeller were conducted on a different day to verify measurement repeatability. Figure 10 shows the performance characteristics as a function of J obtained under the same testing conditions, i.e., a thrust sensor retention spring with stiffness k = 1.50 in./lb and a propeller shaft rotation of 3000 rpm. This test was conducted six days after the completion of the first experiments. The measured tare torque for this test was 0.012 N-m both before and after the experiment. Thus, all three of these tests, conducted under the same operating conditions but at different times, show that the propeller thrust and torque coefficients agree to within ±2.1% and ±3.5%, respectively.

There are several other operational characteristics of the propeller dynamometer system that were found during these tests. The C_T plots shown in Figures 7, 8, and 10 all reveal a tendency of the propeller shaft to "stick" under certain conditions. The smooth decrease in C_T with increasing J becomes more discontinuous between approximately J=0.6 and J=0.8. It is postulated that the dynamic response of the propeller dynamometer is affected by the inherent flow characteristics generated by the four-bladed marine propeller at these J's.

During the propeller performance tests, it was noticed that when the dynamometer system was tapped lightly when operating in the J range under question, different propeller shaft extension equilibrium positions could be obtained. This led to the assumption that internal system friction was adversely affecting the thrust measurements. By varying the wind tunnel flow velocity and dynamometer shaft rpm in such a manner as to not change J, it was possible to vary the resulting extension of the propeller shaft due to the different thrust being generated. (This could also be accomplished by changing the thrust sensor retention spring stiffness.) Further investigation of the advance ratio range J=0.6 to J=0.8 under these new conditions resulted in the same tendency of the propeller shaft to "stick." Because the system has a tendency to "stick" over the same range of J under differing output thrust conditions, and, therefore, differing propeller shaft extensions, it was concluded that the friction experienced was the result of the flow about the propeller coupled to the system. The propeller dynamometer shaft assembly itself was not the cause of this atypical pattern.

Further testing was conducted with the propeller to again verify system repeatability. An LVDT thrust sensor retention spring of stiffness k=1.35 in./lb was used in the next series of experiments. This weaker spring allowed for the same range of J to be examined, as did the k=1.50 in./lb spring, but the LVDT thrust sensor calibration curve was different. Figure 11 shows the results obtained with the k=1.35 in./lb spring. The measured tare torque for this particular test was 0.010 N-m. The tendency of the system to "stick" between J=0.6 and J=0.8 again was evident in the C_T plot, reinforcing the conclusions stated above regarding inherent flow characteristics and system friction.

Finally, Figure 12 shows in summary the measured performance characteristics for "ahead" operation of the Navy #3714 four-bladed marine propeller for every test performed. It should be noted that this data involves tests with varying thrust sensor retention spring constants, varying system tare torque, and varying atmospheric conditions. These composite results reveal that the standard percent difference in the thrust and torque coefficients, as compared to the NSRDC values, for "ahead" operation of the propeller measured were ±5.7% and ±5.3%, respectively. The discrepancy between the mean of the measured efficiency data at any advance ratio value and the NSRDC data is approximately 12%. This is outside the stated measurement error of the dynamometer, which was estimated to be ±4.2% for the efficiency. However, this does not consider the error involved in the NSRDC measurements, which may be approximately ±10%. Part of this difference possibly also can be attributed to the additional power that is required in water to accelerate the "apparent mass" of the water displaced by the propeller to the same advance ratio as compared to in air. We plan to continue to explore the reason for these differences.

"Backing" performance tests were conducted on the propeller on two separate days. A thrust sensor retention spring of stiffness k=1.25 in./lb was utilized in both experiments. Figure 13 shows the backing performance characteristics as a function of J for the first test, while Figure 14 shows the results of the second test. The measured tare torque was 0.015 N-m before and after each test. Following the sign convention of the data provided, the performance characteristics have been plotted in the opposite sense of the data presented for "ahead" operation. The same general trends of C_T, C_Q and h prevail for the "backing" performance although thrust output is degraded as compared to the "ahead" performance and torque required is slightly less.

It can be seen in Figures 13 and 14 that no apparent "sticking" of the propeller shaft occurs over the range of J measured. This reinforces the conclusion that in "ahead" operation inherent flow characteristics affect the dynamometer thrust measurement between J=0.6 and J=0.8. It can also be seen in Figures 13 and 14 that the C_T measurements are slightly more negative (greater) than the Navy data, as was the case for "ahead" performance measurements. This consequently leads to higher values of the efficiency when measured in air.

Flow Visualization Studies:

Kerosene smoke visualization was used to characterize the structure of the flow field about the propeller. This technique has been utilized extensively at the University of Notre Dame and involves the vaporization of kerosene by heating elements within a "smoke generator." The smoke is then pumped into a "smoke rake," in which it cools to ambient temperature and is directed the smoke into the inlet of the wind tunnel. The resulting kerosene smoke tubes are then used to visualize the flow field within the test section. Illustrations of the "smoke generator" and "smoke rake" are shown in Figures 5 and 6. A more complete explanation of the smoke generation process and apparatus is provided by Mueller (1983).

Smoke flow visualization tests incorporated the use of short duration strobe lighting to illuminate the characteristics of the flow in the neighborhood of the propeller. An infrared photo sensor was mounted on one of the aluminum couplings within the dynamometer which is used to trigger several stroboscopes. Three General Radio 1540-P2 Strobolume lamps controlled by three General Radio 1540-P1 Strobolume oscillators connected in series provided sufficient lighting to obtain excellent photographic images of the propeller flow field and wake structure. Each strobe was powered by a General Radio 1540 electronic stroboscope power unit. Synchronizing the strobe flashes with the photosensor also allows for the propeller to appear motionless even while accelerating or decelerating the propeller or wind tunnel free-stream velocity.

Two forms of visual recording media were used to help study the smoke flow visualization, still photographs and real-time video recording. The still camera was a Nikon FM2 35 mm with a 28 mm 1:2.8 lens which was used to record stop-action photographs of the various propeller systems under various conditions. The real-time video recordings were obtained on a Panasonic NV-8950 VCR utilizing a Panasonic HD Digital 5000 WV-S050 motion camera system. Digitization of the video picture at various conditions of propeller operation can also be used to represent the stop-action photography. Real-time video recording allows the investigator the ability to obtain a continuous record of the stroboscopically illuminated images of the flow field. Using

this technique, continuous flow images can be acquired while accelerating or decelerating the flow, thereby providing a continuous record of the flow field over a range of advance ratios. The development of the wake structure is clearly recorded as the propeller changes from one advance ratio to another. For the stop-motion photographs, the strobe lamps were synchronized directly to the Nikon camera to provide a single high intensity flash for each photo. With the ability to extract still pictures from real-time video, through the use of a Data Translation DT2255 Frame Grabber board used in conjunction with a Macintosh II computer, quality "photos" of the flow were obtained. The Frame Grabber board digitizes and stores an image from video signal which can be displayed with square-pixel accuracy on a Macintosh II high resolution computer screen. The photos have also been enhanced through the use of ImageStudio 1.5 software. This software provides the user with the ability to alter a digitized "photo." Contrast enhancement and image sharpening have been used to improve the quality of the pictures for presentation in this thesis. This section will present a few representative "photos" that have been acquired in this manner.

Figures 15, 16,17, and 18 show the typical flow structure at J=0.4, J=0.8, J=1.1 and J=1.2, respectively, for "ahead" performance of the propeller. Figure 15 represents the flow structure characteristic of low J operation of the propeller. The sharply curved smoke streamlines entering the plane of the propeller are a result of flow convergence through the propeller. When the dynamometer system and wind tunnel are operating at steady state conditions, the mass flow rate at any cross-section of the wind tunnel must be a constant. Assuming that the upstream velocity is constant across the wind tunnel cross-section, and because the propeller slip stream velocity is much larger than the free-stream velocity at low J, there must be a component of velocity directed toward the propeller disk area due to the acceleration of the flow which occurs at the plane of the propeller. Also, because the upstream velocity is small, the relative angle of attack of the incoming flow seen by the propeller blades is large. As with any airfoil section, excessively large angles of attack are met with flow separation and transition to turbulent flow. These phenomena are depicted by the disturbed wake seen behind the propeller.

Figure 16 represents the "ahead" operation flow characteristics for a propeller efficiency of approximately $\eta=0.70$ at J=0.8. Although the wake structure of the propeller is seen to be much more defined than in Figure 15, which is the result of little or no flow separation from the propeller blades, losses in efficiency still occur because of the formation of propeller tip vortices. These losses are analogous to the induced flow caused by tip vortices of a finite wing. Less curvature of the incoming streamlines is also revealed in Figure 16, a result of the higher free-stream velocity encountered at higher J. It should also be noted that the propeller blade passage "cuts", seen directly below each vortex structure, are somewhat parabolic in shape. This reveals that the propeller blade is not generating as much thrust at the blade root and tip as it is in the blade middle regions. Uniform blade loading would yield a "cut" parallel to the plane of the propeller blades. The propeller blade is not evenly loaded, resulting in less than maximum efficiency.

Figure 17 shows the propeller operating at its most efficient conditions (J=1.1). Incoming smoke streamlines are seen to be completely perpendicular to the plane of the propeller and very small tip vortices are evident reflecting minimized tip effect losses. The propeller blade passage "cuts," seen directly below each vortex, also reveal a uniformly loaded propeller. This shows that each section of the propeller blade is generating an equal amount of thrust.

Figure 18 shows the flow characteristics for the propeller operating at an efficiency of approximately $\eta=0.83$ at J=1.2. The very low relative angle of attack of the free-stream flow seen by the propeller blades results in a loss of thrust at this high J. Both minimal tip effect losses and an evenly loaded propeller are again evident in Figure 18, as they were in Figure 17, but with the relative angle of attack of the free-stream converging on the cord line of the propeller blades, less thrust is being developed.

These visualization techniques can be extended to elucidate greater detail in flow structure, such as the flow separation and the fine structure and spacing of the tip vortices. Examples of this are shown in Figures 19, 20 and 21 for the four-bladed marine propeller. Figures 19 and 20 show frontal views of "ahead" propeller operation at J=0.3 and J=0.8, respectively. Flow separation at the blade of the propeller is seen in the low advance ratio "photo" (Figure 19) and the three

dimensionality of the flow structure is clearly seen in the J=0.8 "photo" (Figure 20). Figure 21 reveals how the tip vortices are formed and shed parallel to the angle of the propeller blade tip. The ability to correlate propeller performance measurements with flow structure visualization makes the new propeller dynamometer a very useful tool.

c. Plans for Next Year's Research

We plan to continue to use the advanced dynamometer with the objective to incorporate it into our studies of the effect of variable inflow conditions in which the fluid mechanical and acoustic characteristics of the flow field. To this end, we plan to begin the third stage of our research, in which the rotor is operated in a duct. Once this is completed, we plan to begin the fourth stage, in which the effect of upstream turbulence intensity (between 0.07% and 5.0%) on performance will be determined, and acoustic measurements will be made to ascertain the influence of the turbulence length scale at the same intensity and its relation to the radiated noise spectrum.

II. WIND TUNNEL/ACOUSTIC FACILITY

a. Description of Research

In order to prepare for the acoustic measurements to be made, two studies were performed: 1.) modification of one of the existing low turbulence, closed test section wind tunnels and 2.) the design of a new low-noise low-turbulence, free-jet wind tunnel. The design criteria included a free jet-anechoic chamber facility with a low turbulence (i.e. 0.07%) uniform flow (maximum velocity of 100 ft/sec) with a cross-section of approximately four square feet and the low frequency cut off of approximately 150 Hz.

b. Significant Results since 1 April 1989

Modifications to one of the existing wind tunnels would require a new diffuser with a muffler and an anechoic chamber. Because of space limitation only a very small anechoic chamber could be built. The opportunity to design and build a new facility presented itself when the University decided to make a new home for the Aerospace Research Laboratory. The design studies for the inlet, anechoic chamber, and diffuser began in mid-July. Visits were made to the aeroacoustic wind tunnel facilities at NASA Lewis Research Center and General Electric Company, Evandale, Ohio to discuss wind tunnel design and acoustic measurement techniques.

Working with the architects for the new Aerospace Research Laboratory and Eckel Industries, Inc., an anechoic chamber was designed. This will have a working space 20 ft wide by 26 ft long by 8 ft high with 22 in. fiberglass sound absorbing wedges on all six sides. This wedge configuration will provide a low frequency cutoff of 150 Hz. Above the cutoff frequency, the wedges will have a coefficient of energy absorption at normal incidence equal to 0.99 or greater. A low turbulence subsonic free-jet/closed test section wind tunnel was also designed. This will fit into the anechoic chamber for aerodynamic measurements of sound pressure level and sound intensity generated from propellers, airfoil configurations, etc. The cross-sectional area of the tunnel test section will be four square feet with a maximum velocity of approximately 100 ft/s. The tunnel has been designed so that it can be removed from the chamber to accommodate other acoustic experiments. The floor plan of the anechoic facility and wind tunnel are shown schematically in Figure 22.

c. Plans for Next Year's Research

Construction drawings of the new free-jet/closed test section wind tunnel facility will be completed and the fabrication of components will begin. Plans are being made so that the wind tunnel can be incorporated into the new Aerospace Research Laboratory and be ready in early

Spring 1991. Pilot experiments using one of our existing wind tunnels to develop inflow measurement techniques will continue.

III. FLUID DYNAMIC & ACOUSTIC MEASUREMENTS

a. Description of Research

Turbomachine rotors usually are located where the approaching flow is nonuniform. As a result, the rotor blades are subject to fluctuating forces that are induced by the irregular and unsteady inflow patterns. This causes vibration of the rotor and its associated structure and produces the radiation of unwanted noise. Because it is not possible with present technology to eliminate rotor inflow nonuniformities, it is therefore important to determine the rotor's response in terms of the fluid mechanical and acoustic characteristics of the flow field both upstream and downstream of the rotor. To this end, experiments will be conducted in which the flow field's mean velocities, fluctuating components and spectra, and resultant sound intensities of the radiated noise are measured. These measurements will be conducted in conjunction with flow visualization studies aimed at identifying possible flow structures responsible for noise at selective frequencies. Simultaneous measurements of rotor performance also will be made.

b. Significant Results since 1 April 1989

Initial flow visualization studies have been conducted during the rotor-dynamometer shakedown tests and have ascertained that it is possible with our present system to clearly identify flow structures about the blade's surfaces, as described in section I. The goal using this approach is to identify what flow structures (e.g., separated regions along the blade's surface) contribute to degradation in rotor performance and. possibly, any resulting unwanted noise. In this manner, regions of interest can be identified for subsequent detailed flow and blade surface measurements.

Preliminary acoustic measurements were performed in our existing wind tunnel facility to study the influence of upstream turbulence intensity. The measurements were carried out using two phase-matched 0.5 in. microphones separated by a 12 mm spacer in the range of 0 to 4000 Hz in six octave bands. This is because the propeller noise is comprised of two components; one, a discrete low frequency contribution that results from the rotation of the blades, and, the other, a broadband contribution that results from turbulence and wake effects. The data obtained from these measurements currently is being analyzed.

c. Plans for Next Year's Research

The accuracy of the twin-microphone technique will continue to be studied. If this approach is deemed appropriate after several benchmark tests, this technique will be applied in a series of initial experiments to determine the influence that the intensity and scale of the inflow turbulence has on the radiated noise. In addition, detailed flow visualization and fluid dynamic flow field characterization studies will be conducted coupled with the rotor performance measurements.
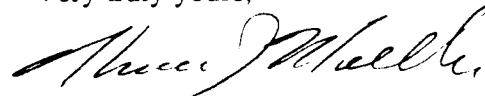
REFERENCES

1. Asson, K.A., "The Development of an Advanced Dynamometer System to Experimentally Determine Propeller Performance," M.S. Thesis, Department of Aerospace & Mechanical Engineering, University of Notre Dame, May, 1990.

2. Mueller, T. J., "Flow Visualization by Direct Injection," Chapter 7, pp.307-375, Fluid Mechanics Measurements, Washington D.C., Hemisphere Publishing Co, 1983.

3. Mueller, T. J., "Smoke Visualization of Subsonic and Supersonic Flows (The Legacy of F.N.M. Brown)," Final Report UNDASTN-34121, AFSOR-TR-78-1262, June 1978.

CONCLUDING REMARKS

All phases of this project are on schedule at the present time. During the next year, the major effort will be to include the variable inflow conditions i.e., effect of upstream turbulence intensity and scale. The techniques necessary to obtain detailed flow visualization, fluid dynamics and acoustic properties of the propeller flowfields will continue to be developed. Performance studies with and without the propeller duct will also be made. Further analysis of all data will be performed to determine where further efforts need to be concentrated.

Very truly yours,

Thomas J. Mueller, Ph.D.
Roth-Gibson Professor of
Aerospace Engineering

Patrick F. Dunn, Ph.D.
Associate Professor, Aerospace
and Mechanical Engineering

cc: Dr. F. M. Kobayashi
       Dr. A.N. Michel
       ONR Regional Office (1)
       NRL (6)
       DTIC (12)
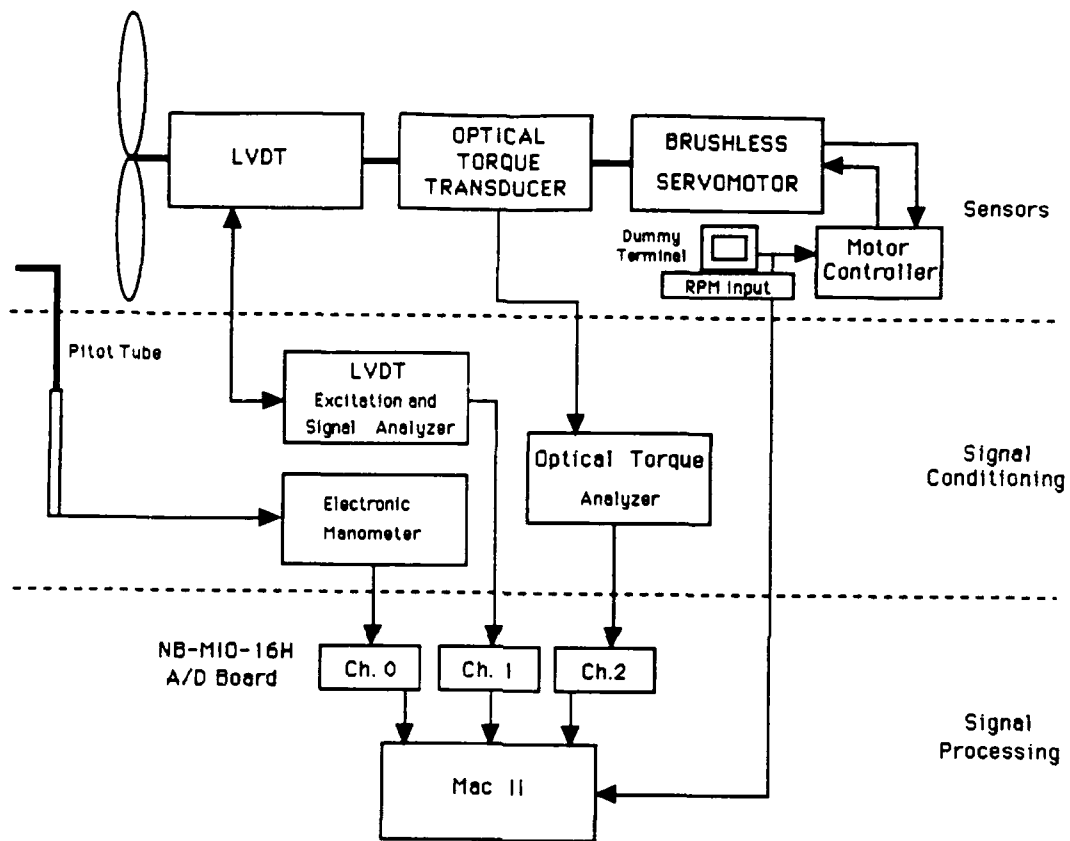
Figure 1 Schematic Drawing of the New Propeller
Dynamometer Measurement System
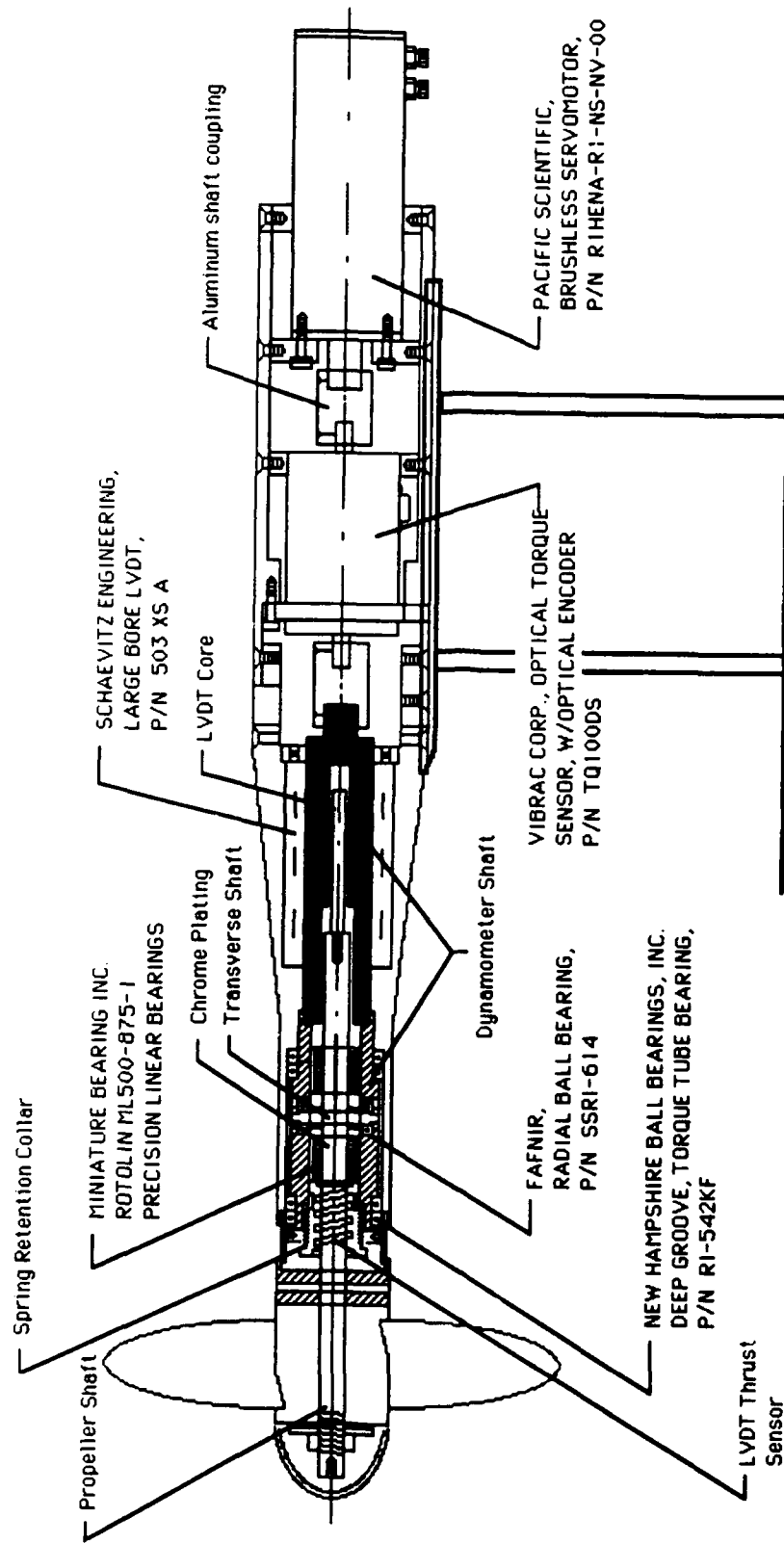
Figure 2 Detailed Drawing of the New Propeller Dynamometer Measurement System

Dynamometer Shaft
Assembly

New Hampshire RI-542KF
Deep Groove Torque Bearings

Race for Fafnir Radial Bearings

Phenolic Dynamometer
Shaft Extension

Miniature Bearing Inc.
Rotolin ML500-875-1
Precision Linear Bearings

Propeller Shaft
Assembly

Chrome Plating

Spring
Retension
Collar

Transverse Shaft

Fafnir SSRI-614
Radial Bearings

Locking
Nut

LVDT Core
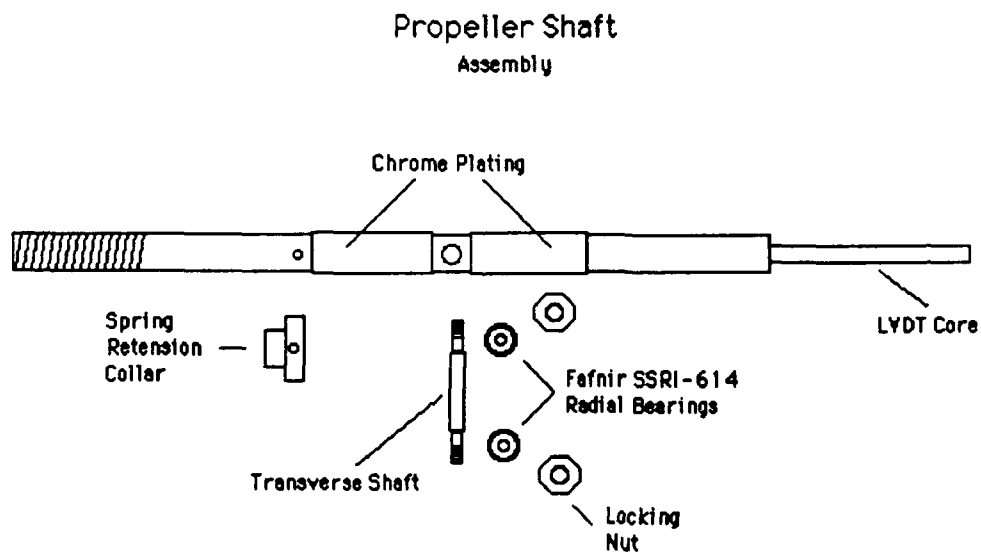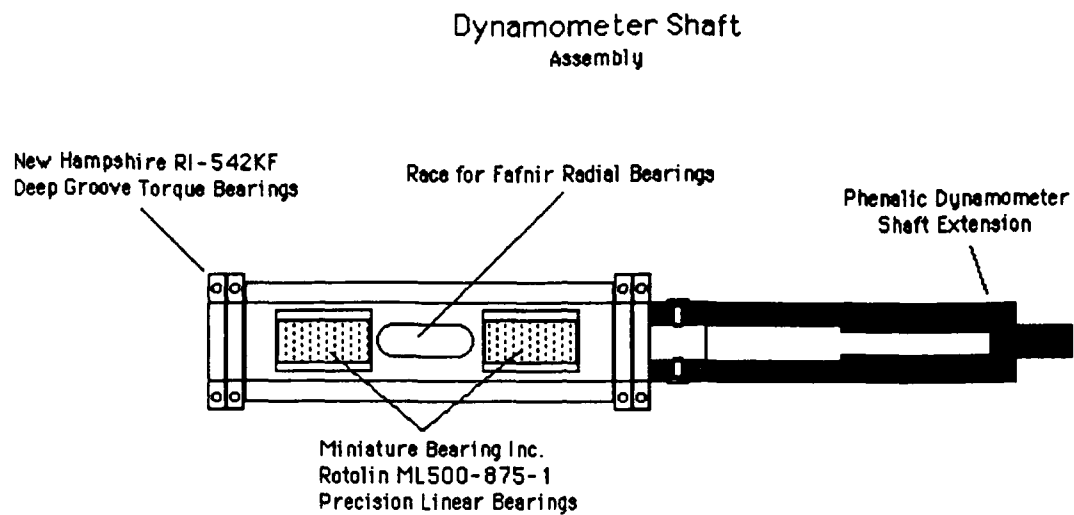
Figure 3 Detailed Drawing of the Dynamometer Shaft
Assembly and Propeller Shaft Assembly
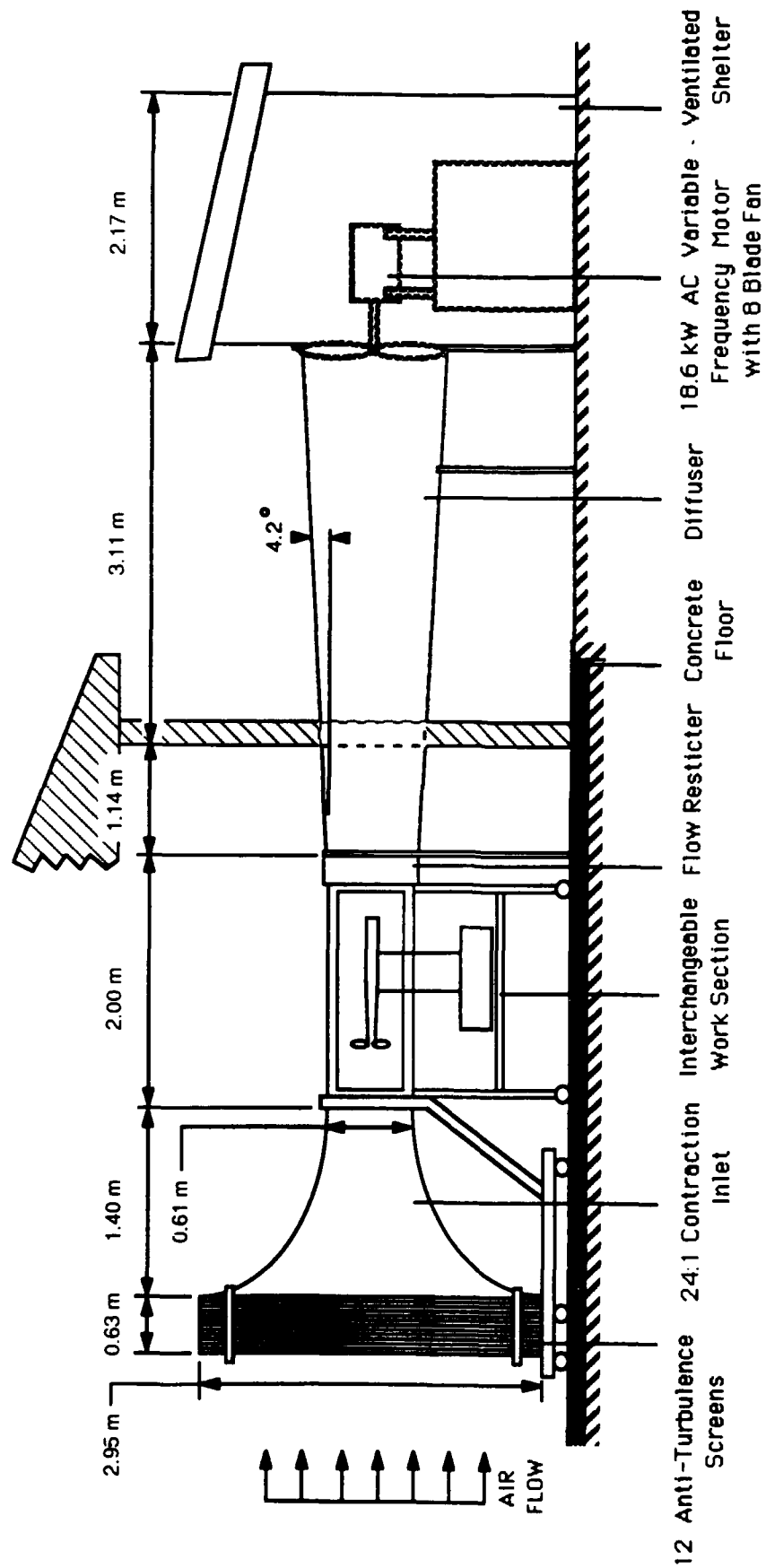
Figure 4 Wind Tunnel Facility
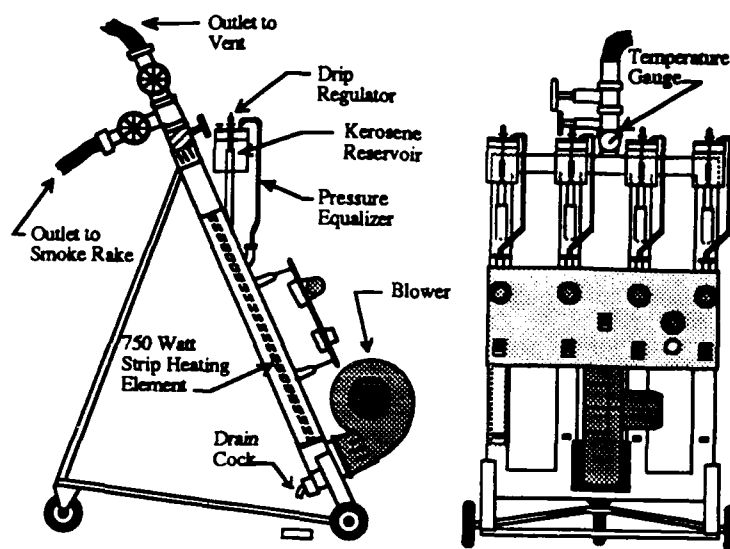
Figure 5 Kerosene Smoke Generator
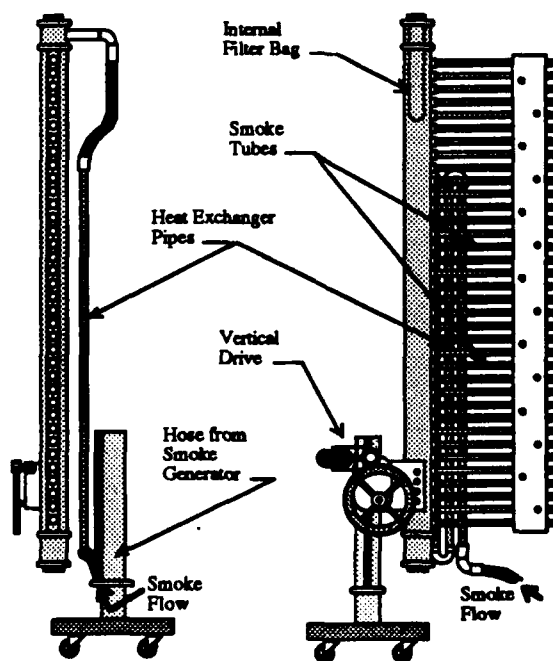
Figure 6 Kerosene Smoke Rake
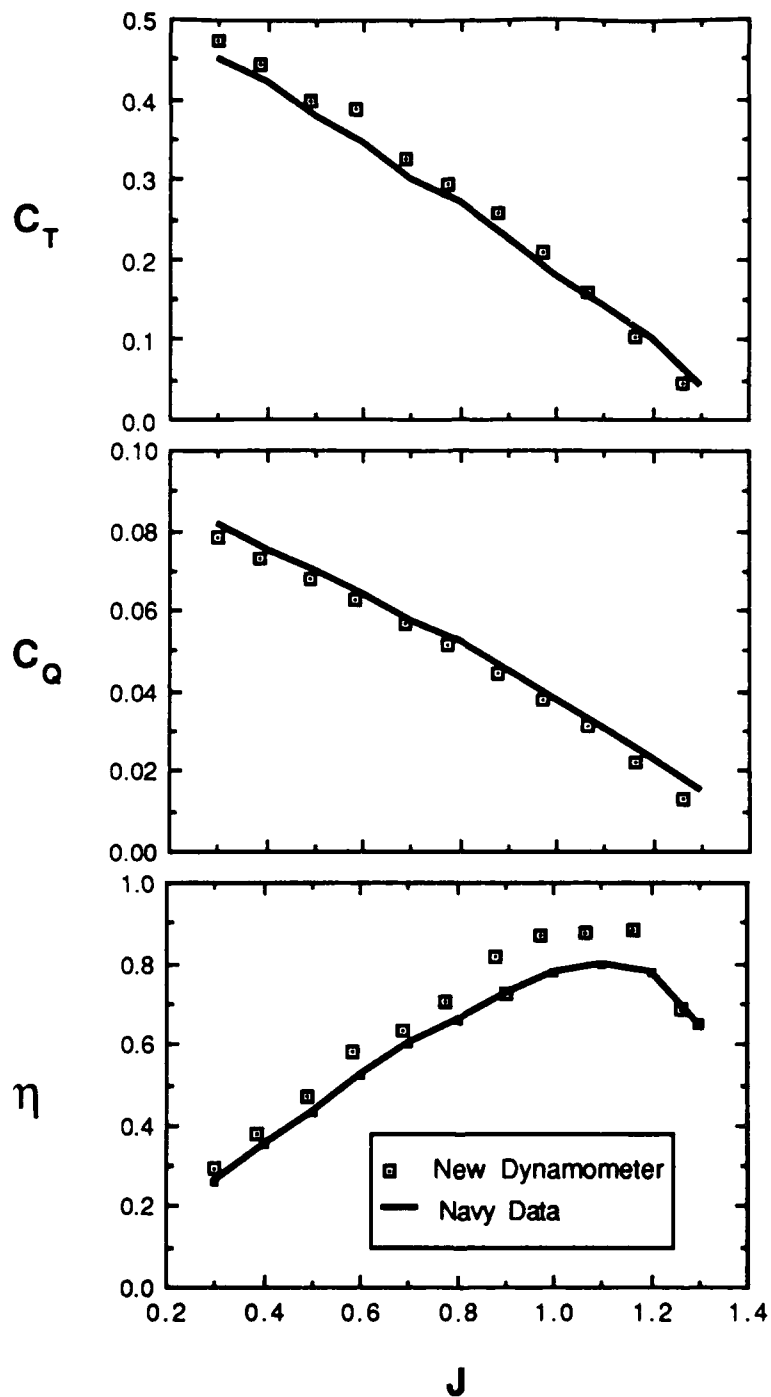
Figure 7   Navy #3714 Ahead Propeller
          Performance Coefficients vs J
          (First Test Conducted in Series of Three)
          (Thrust Retention Spring k=1.50 lb/in.)
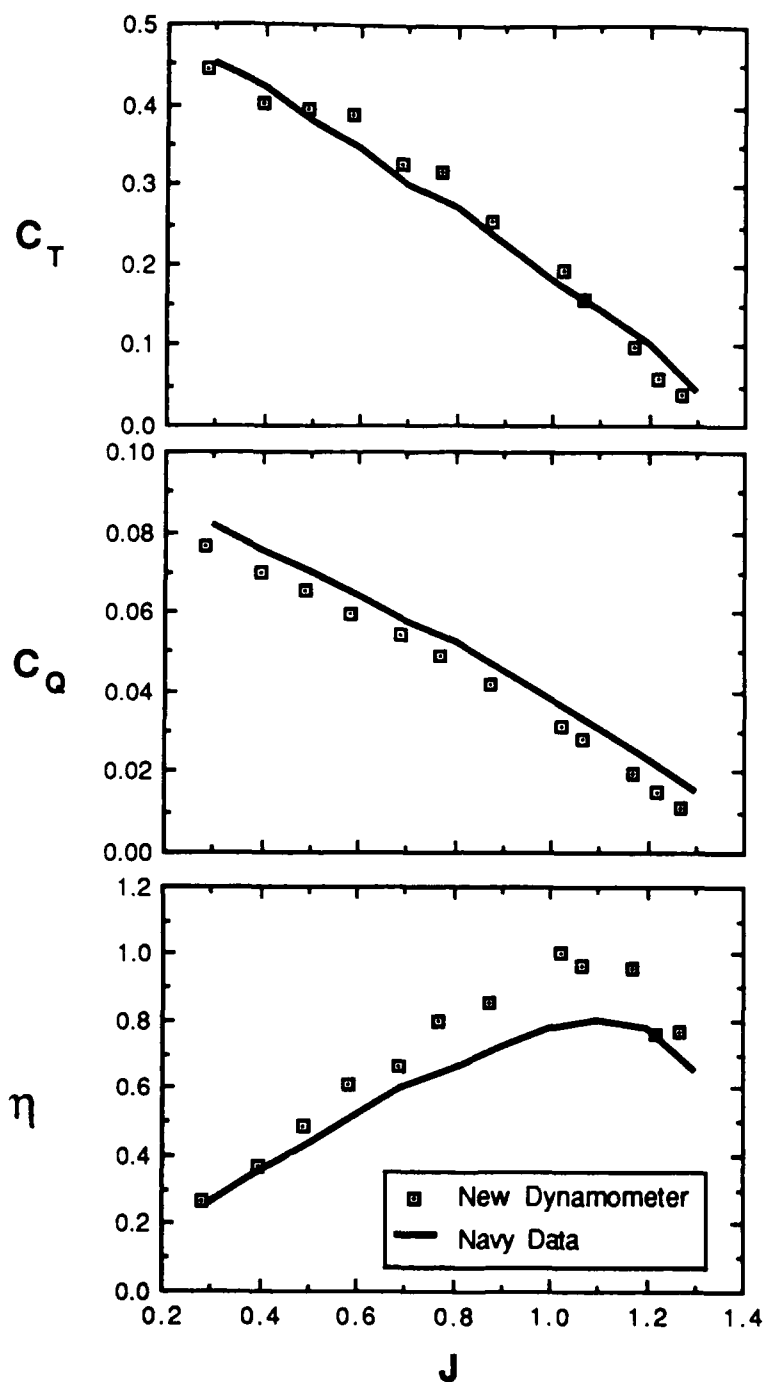
Figure 8 Navy #3714 Ahead Propeller
Performance Coefficients vs J
(Third Test Conducted in Series of Three)
(Thrust Retention Spring k=1.50 lb/in.)
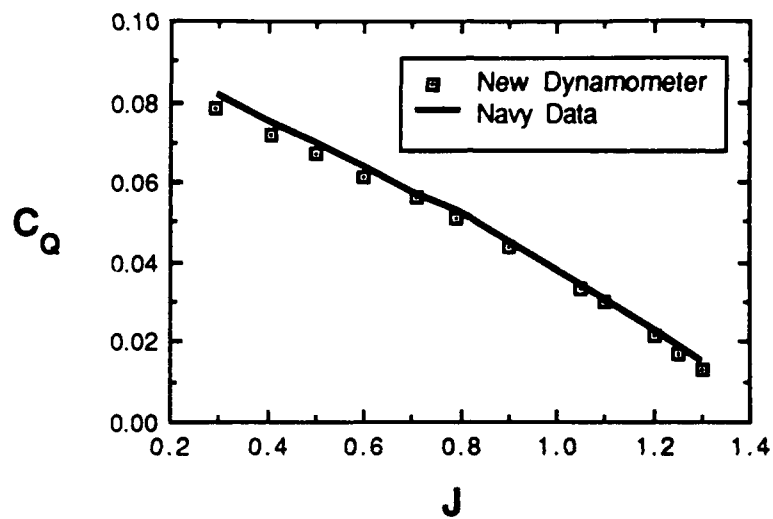
Figure 9   Navy #3714 Ahead Propeller Torque
Coefficient vs J Using Corrected Tare
Torque Values
(Thrust Retention Spring k=1.50 lb/in.)
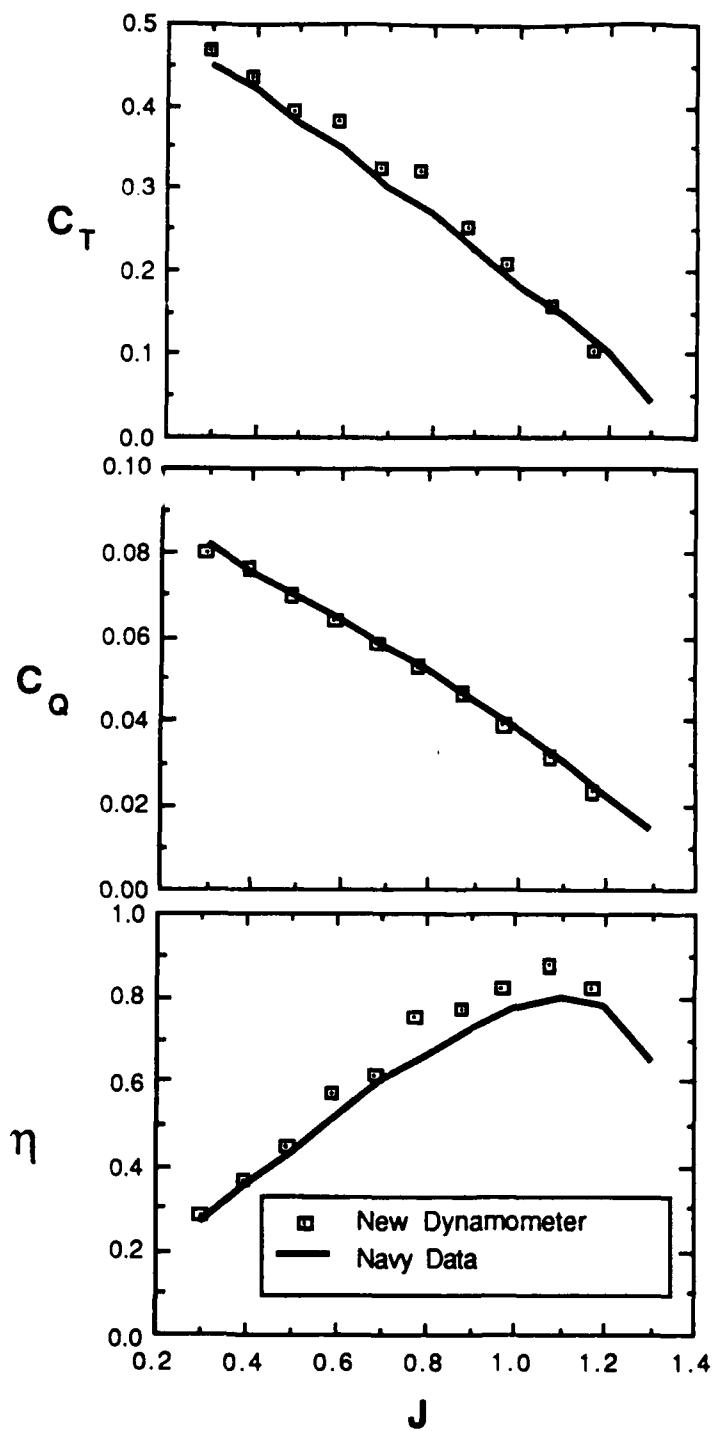
Figure10 Navy #3714 Ahead Propeller
Performance Coefficients vs J
(Conducted Six Days After First Tests)
(Thrust Retention Spring k=1.50 lb/in.)
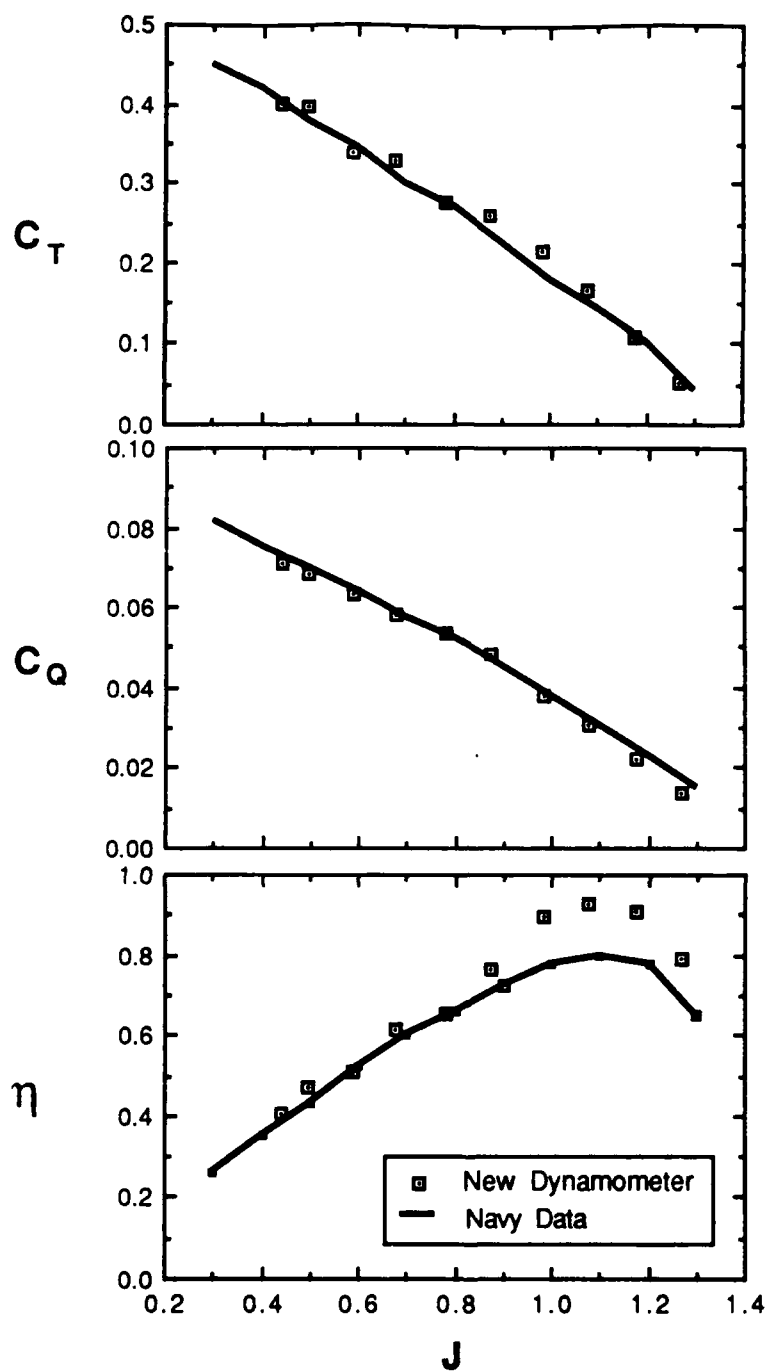
Figure 11 Navy #3714 Ahead Propeller
Performance Coefficients vs J
(Thrust Sensor Retention Spring k=1.35 in/lb)
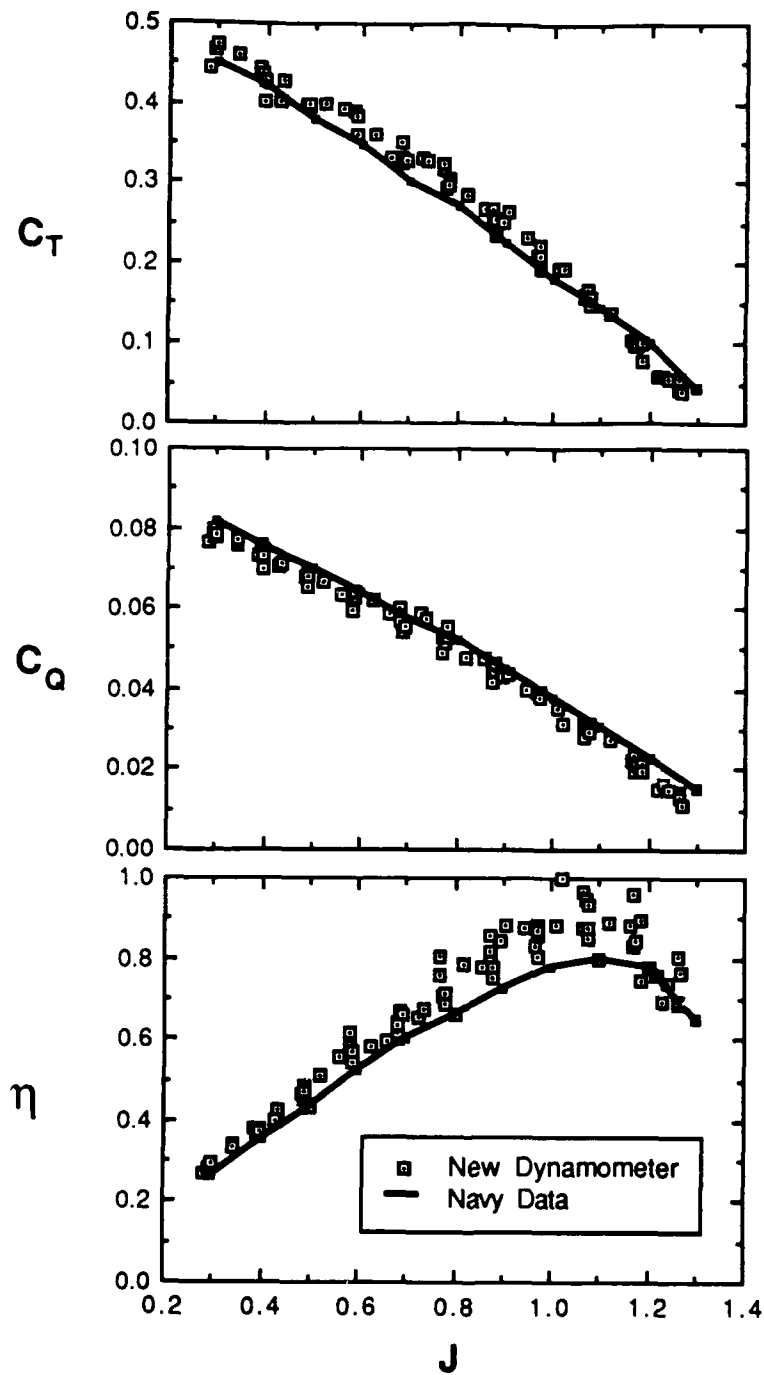
Figure 12 Navy #3714 Ahead Propeller
Performance Coefficients vs J
(All Tests Combined)
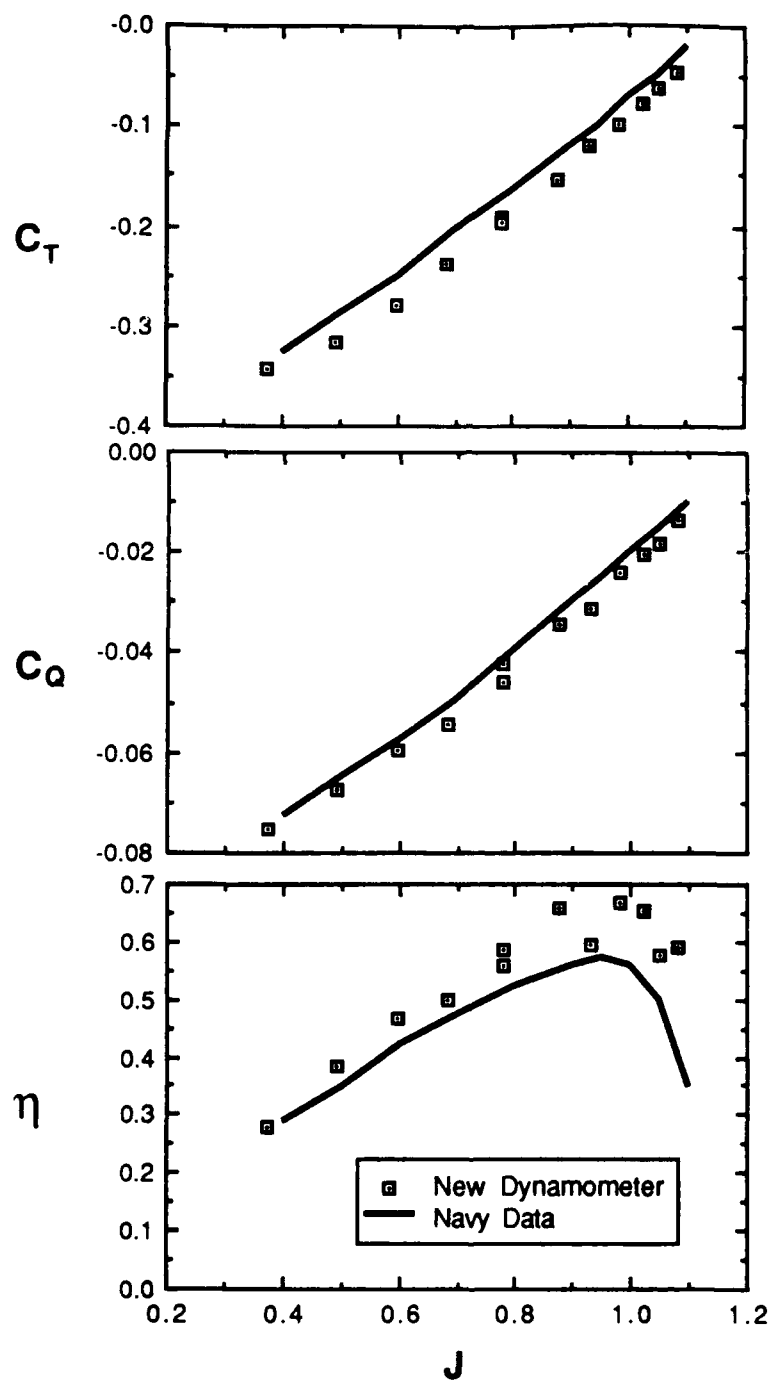
Figure 13 Navy #3714 Backing Propeller
Performance Coefficients vs J
(First Test Conducted)
(Thrust Sensor Retention Spring k=1.25 lb/in.)
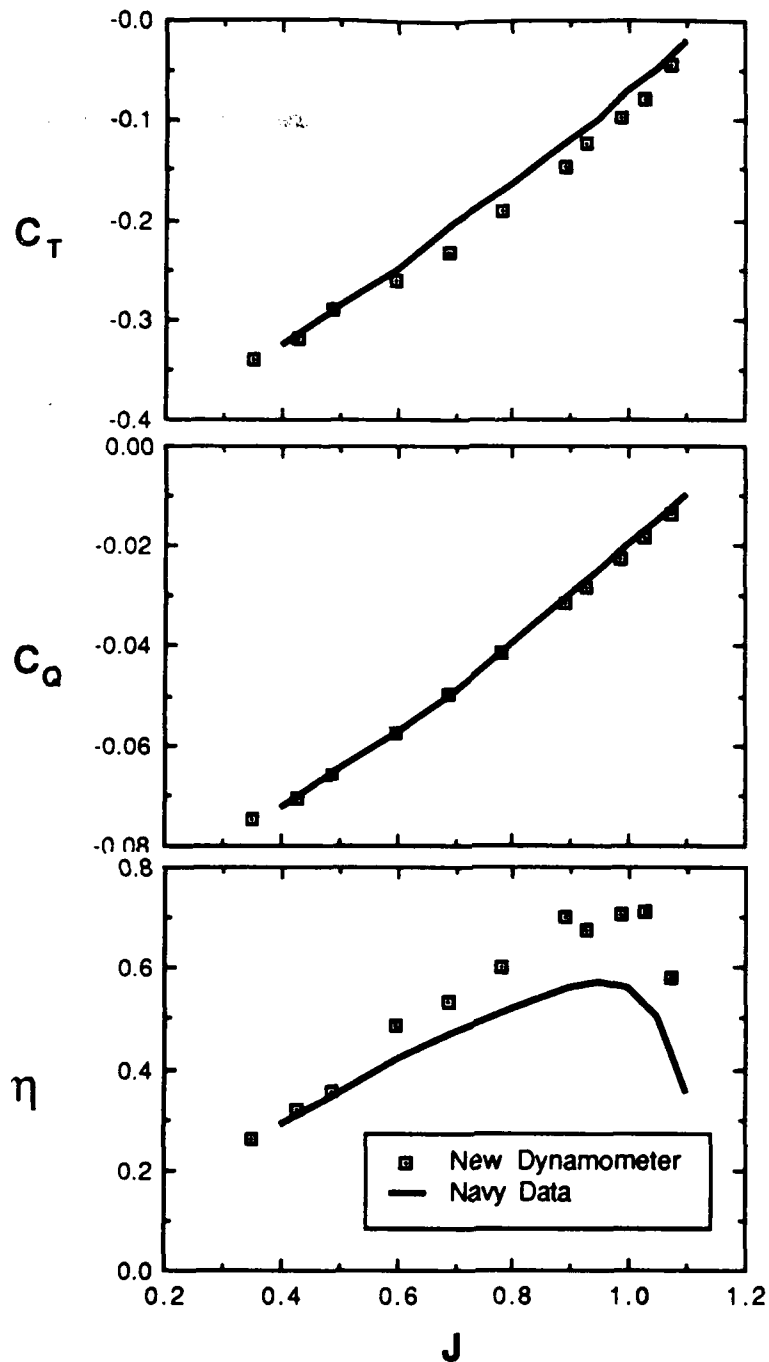
Figure 14 Navy #3714 Backing Propeller
Performance Coefficients vs J
(Second Test Conducted)
(Thrust Sensor Retention Spring k=1.25 lb/in.)
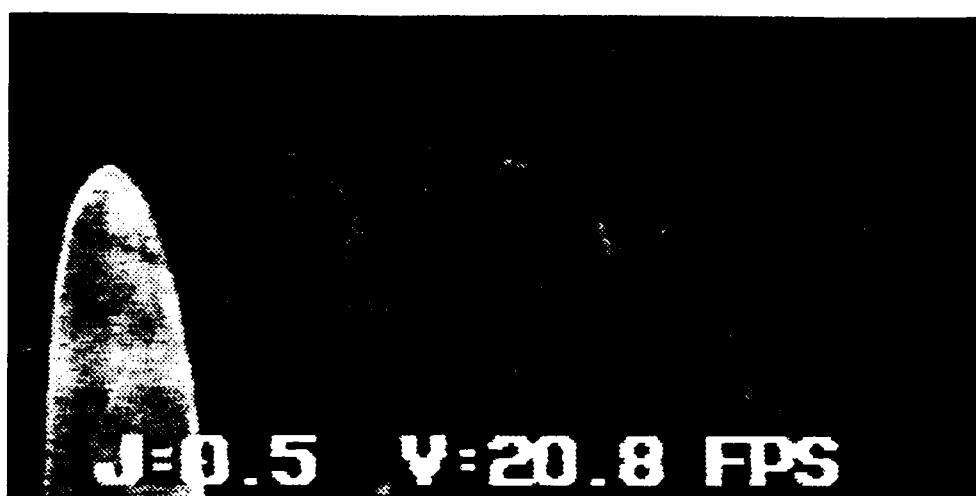
Figure 15 Navy #3714 Ahead Operation Kerosene Smoke
Flow Visualization. J=0.5
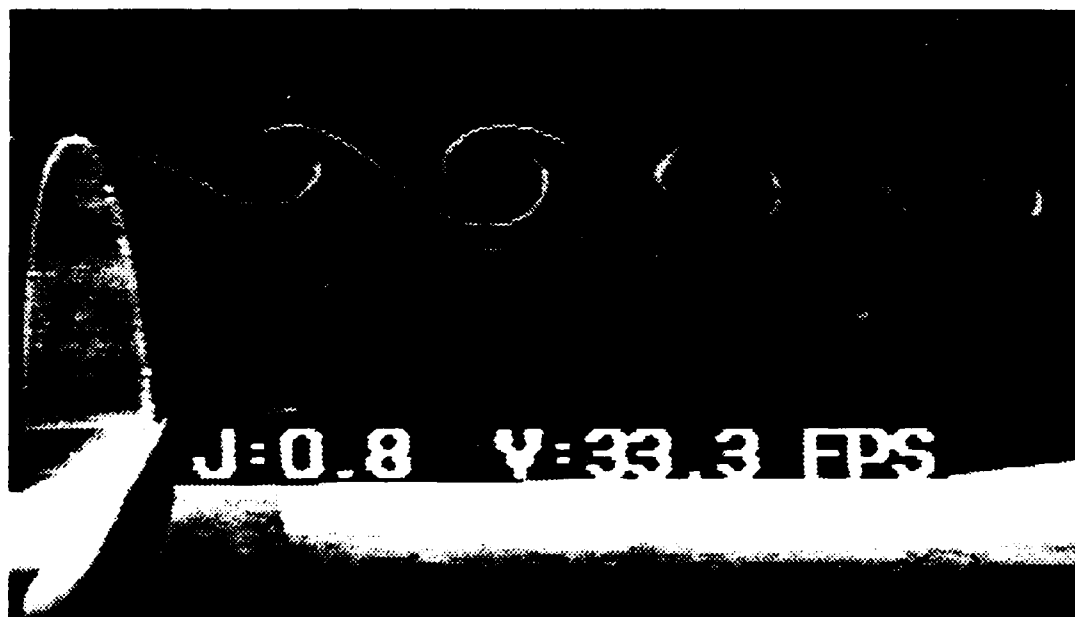
Figure 16 Navy #3714 Ahead Operation Kerosene Smoke
Flow Visualization. J=0.8
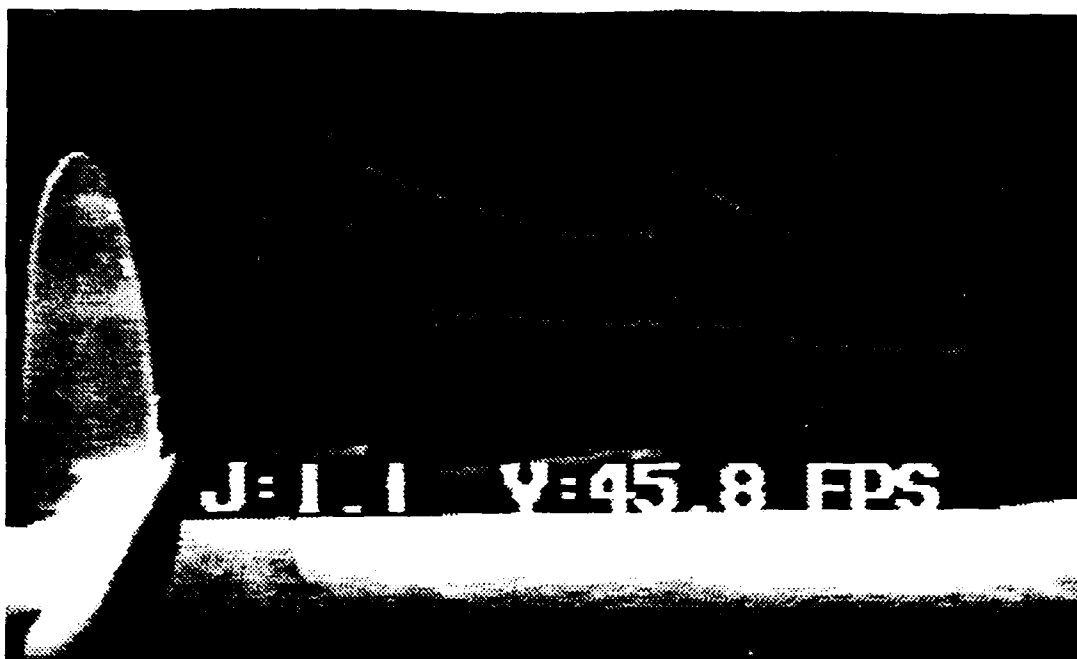
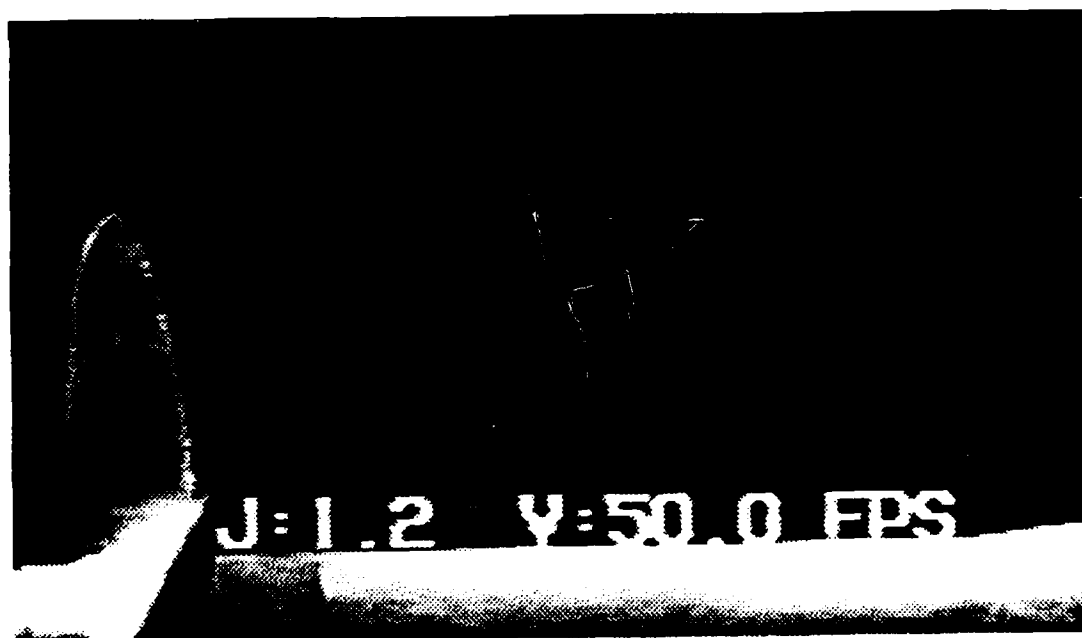Figure 17   Navy #3714 Ahead Operation Kerosene Smoke
Flow Visualization. J=1.1

Figure18   Navy #3714 Ahead Operation Kerosene Smoke
Flow Visualization. J=1.2

Figure 19 Navy #3714 Ahead Operation Kerosene Smoke
Flow Visualization. J= 0.3   Frontal View

Figure 20 Navy #3714 Ahead Operation Kerosene Smoke
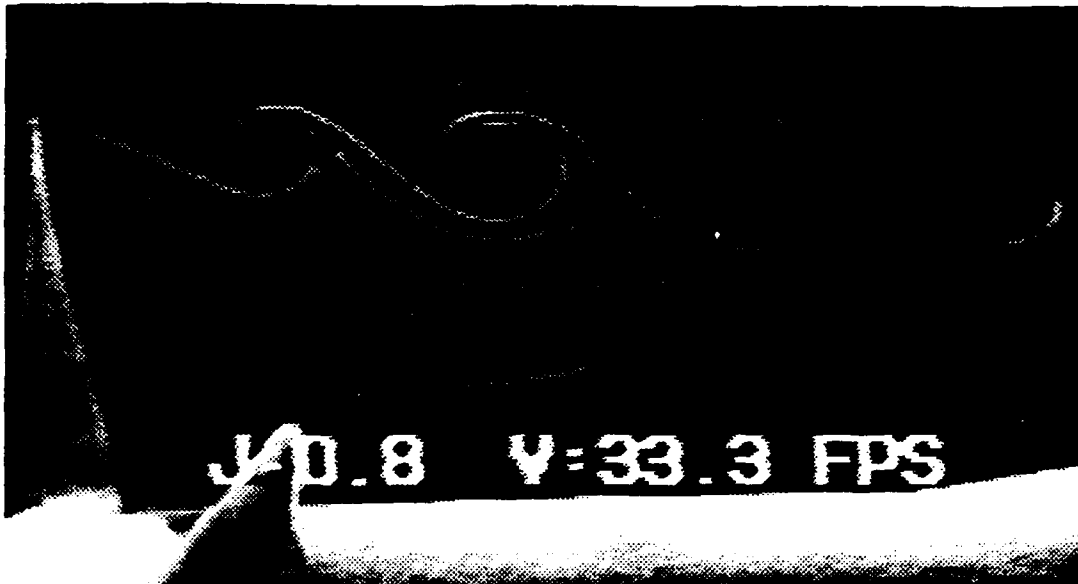Flow Visualization. J=0.8 - Frontal View

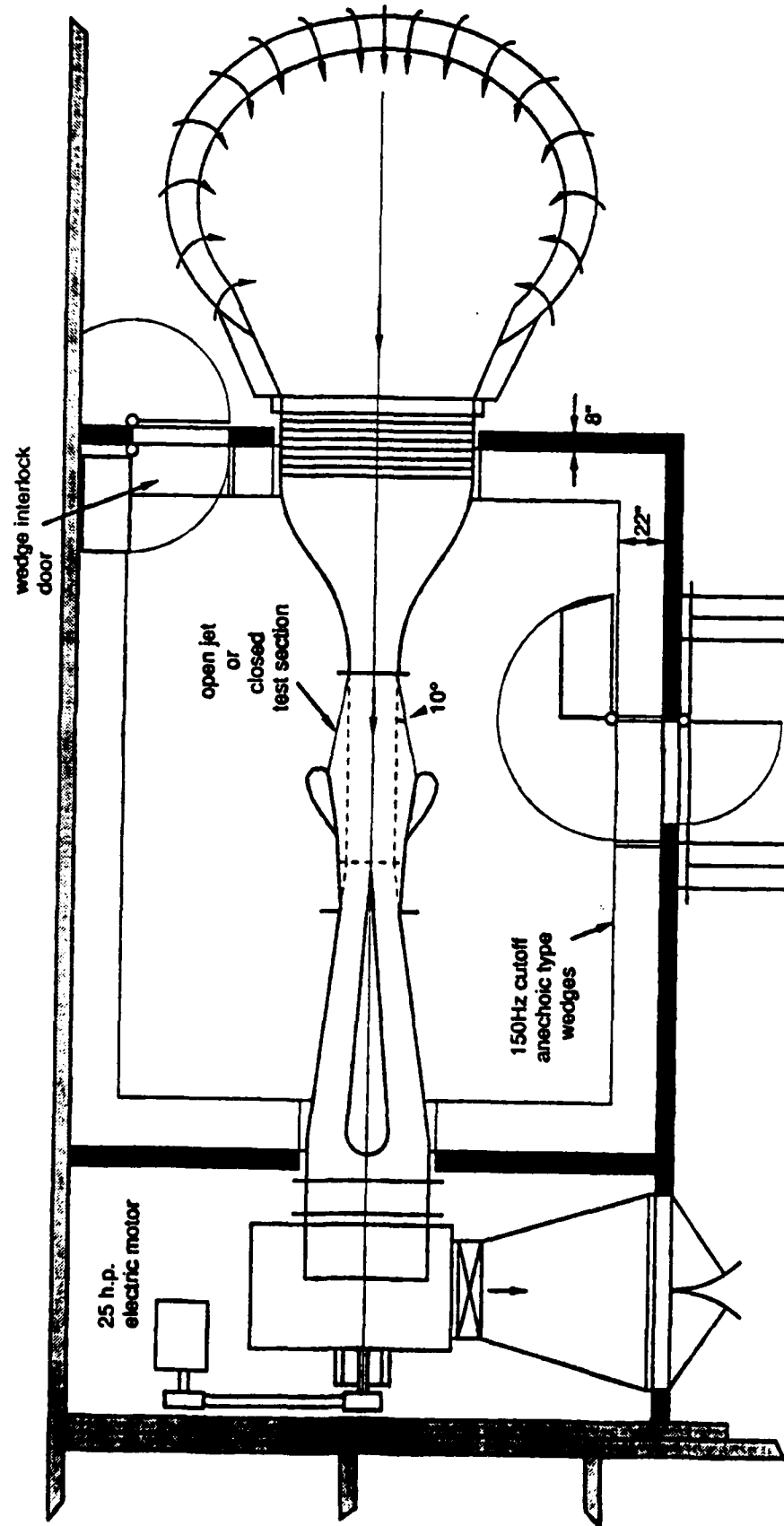Figure 21   Navy #3714 Ahead Operation Kerosene Smoke
Flow Visualization. J=0.8 - Blade Angle View

Figure 22   Anechoic Flow Facility